INORGANIC CHEMISTRY FRONTIERS

CHINESE CHEMICAL SOCIETY | ROYAL SOCIETY OF CHEMISTRY

RESEARCH ARTICLE

View Article Online
View Journal | View Issue

Cite this: *Inorg. Chem. Front.*, 2021, **8**, 2771

Raman and optical characteristics of van der Waals heterostructures of single layers of GaP and GaSe: a first-principles study†

Yigit Sozen[a] and Hasan Sahin *[a,b]

Received 11th February 2021,
Accepted 30th March 2021

DOI: 10.1039/d1qi00187f

rsc.li/frontiers-inorganic

One of the effective methods to modulate or improve the fundamental properties of 2D van der Waals materials is building their heterostructures. In this study, we employ first-principles calculations based on density functional theory to predict the ground state properties of vertically aligned single layer crystals of GaP and GaSe. First, it is shown that, depending on the intimate contact atoms in GaP, the crystal formation of heterostructures displaying characteristics of type-I and type-II heterojunctions is possible. Here, the quasiparticle bandgaps for the spatially direct and indirect electronic transitions are calculated to be 2.70 and 1.78 eV, respectively. Vibrational analysis not only reveals the dynamic stability of the heterostructures but also allows the calculation of the Raman activity spectrum of each structure, providing a fingerprint of the stacking type. In addition, by solving the BSE equation on top of G_0W_0 approximation, the optical gaps, reflectance and transmittance spectra of the heterostructures are determined. The calculated absorption spectra demonstrate that the spectral position and characteristics of the optical transitions are altered depending on the heterojunction type. Furthermore, it is found that the interband and intraband transitions in the GaP/GaSe heterostructures can also be monitored *via* their reflectance and transmittance spectra.

1 Introduction

Following the appearance of graphene,[1,2] two-dimensional (2D) van der Waals structures have become one of the desirable classes of materials for optoelectronic applications,[3–7] due to their potential advantages of being able to integrate them in nano-sized devices[8] and their scalable intrinsic properties.[9,10] So far, large-scale atomically thin forms of 2D materials have been mostly synthesized by performing experimental techniques such as mechanical exfoliation[11–13] and chemical vapor deposition.[14–18]

Among the semiconducting materials, the binary compounds of group III–V elements have particularly been used in light-based device applications[19–25] over the last 50 years, owing to their remarkable optical properties such as high photoresponses,[26,27] strong light emission,[28,29] and high carrier mobility.[30–33] In addition, theoretical studies have revealed that the 2D honeycomb structures of group III–V binary compounds can be stabilized even in their free-standing one-atom-thick form.[34] However, in experimental conditions, the cleavage of these compounds into the 2D form remains challenging due to the covalent nature of their bulk counterparts, which has led researchers to develop more convenient growth techniques for non-layered structures instead of traditional ones. However, a very recent study has reported that 2D ultra-thin single crystals of GaP, GaN, GaSe, InP and InSe can be successfully synthesized.[35] As a photonic material, bulk and nano-sized GaP has been widely used in light-producing applications due to its superior optical properties,[36–40] however, studies on its atomically thin form, which has been reported to be a wide band gap semiconductor, are still insufficient.[34,41] As a result of the rapid developments in the field of ultra-thin materials, the search for their potential applications continues rapidly.

Group III monochalcogenides are another group of 2D materials composed of vertically aligned tetralayered slabs containing pairs of metal and chalcogen atomic planes. Among them, bulk GaSe is a semiconductor with a direct band gap of 2 eV which possesses nonlinear optical properties related to its crystal symmetry.[42,43] Thus far, various growth methods have been reported for the large-scale synthesis of few-layer and monolayer GaSe.[44–48] It has been shown that decreasing the layer number results in a direct-to-indirect band gap transition

[a]*Department of Photonics, Izmir Institute of Technology, 35430 Izmir, Turkey. E-mail: hasansahin@iyte.edu.tr*
[b]*ICTP-ECAR Eurasian Center for Advanced Research, Izmir Institute of Technology, 35430 Izmir, Turkey*

†Electronic supplementary information (ESI) available. See DOI: 10.1039/d1qi00187f

Published on 31 March 2021. Downloaded by Izmir Yuksek Teknoloji on 5/6/2022 8:51:36 AM.

View Article Online

Published on 31 March 2021. Downloaded by Izmir Yuksek Teknoloji on 5/6/2022 8:51:36 AM.

in GaSe being demonstrated.[49,50] In addition, the band gap of ultra-thin structures of GaSe can be modulated *via* compressive or tensile strain.[51,52] Various studies have demonstrated that ultra-thin GaSe crystals can be integrated for a variety of device applications such as optoelectronics, by virtue of their superior features such as a high photoresponse,[44,46,53] high piezo-phototronic response,[54] and large second-harmonic generation intensity.[55]

Constructing van der Waals heterostructures of ultra-thin materials is an efficient technique for obtaining desired electronic and optical properties.[56–59] To date, the synthesis of heterostructures composed of TMDs has been reported in particular. It has been shown that the combination of MoS_2 and WS_2 single layers, forming a type II heterojunction, enables ultra-fast hole transfer in less than 50 fs from the MoS_2 to the WS_2 layer.[60] Furthermore, interlayer exciton formation with a long recombination life-time (~1.8 ns) was demonstrated in a $MoSe_2/WSe_2$ heterostructure as a consequence of the confined electron and hole states within the separated layers,[61] that allows the material to be used in excitonic based devices.[62–64] Moreover, the formation of a vertically aligned heterojunction of few-layered GaSe and MoS_2, which presents a wide-range photoresponse to wavelengths between the visible and near-infrared areas of the spectrum in the absence of applied voltage, has been demonstrated.[65] In addition, the structure formed by the deposition of GaSe on graphene has been shown to exhibit a fast photoresponse by preventing the formation of trap states within the junction interface.[66]

The paper is organized as follows: details of the computational methodology are given in section 2, the single layer forms of the GaP and GaSe crystals and their energetically favorable heterostructures are investigated in terms of their structural and vibrational properties in sections 3.1 and 3.2, respectively, the electronic and optical properties of the heterostructures are discussed in section 3.2.2 and finally, the conclusions are given in section 4.

2 Computational methodology

First-principles calculations are employed based on density functional theory as implemented in the Vienna *ab initio* simulation package (VASP)[67,68] in order to investigate the structural, electronic, vibrational and optical properties of the GaP and GaSe single-layers, and their vertical heterobilayers. Projector augmented pseudopotential datasets are used for the effective potentials of the core and valence electrons.[69,70] Electronic exchange and correlation interactions are obtained from the generalized gradient approximation (GGA) of the Perdew–Burke–Ernzerhof (PBE) functional.[71] Van der Waals type weak interactions are treated by introducing the DFT-D3 method including the Becke–Johnson damping function.[72] For better approximation of the electronic band gaps, which are underestimated by bare DFT functionals, Heyd–Scuseria–Ernzerhof (HSE06)[73] and G_0W_0 [74–76] corrections are applied including spin–orbit coupling (SOC). To suppress the long-range interactions between repeating layers, the lattice vector vertical to the basal plane of the 2D structures was adjusted to 20 Å.

By using the automatic mesh method, the Brillouin zone (BZ) was subdivided with a 10 × 10 × 1 Γ-centered *k*-point mesh. The cut-off parameter for the kinetic energy of the plane-wave basis set was taken as 400 eV. The volume of the cell was optimized until the total pressure was less than 1 kbar. For phonon calculations, the electronic self-consistent loop was carried out until the energy variation between the consecutive steps became 10^{-8} eV. The cohesive energy per atom (E_{Coh}) was calculated using the equation below:

$$E_{\mathrm{Coh}} = \left[\sum_i n_i E_i - E_{\mathrm{crystal}}\right] / \left[\sum_i n_i\right] \tag{1}$$

where i refers to the atomic types and n_i, E_i and $E_{crystal}$ stand for the number of same type atoms per unit cell, the free energy of the ith atom in a vacuum and the ground state energy of the crystal structure per unit cell, respectively.

Phonon band dispersions are obtained utilizing PHONOPY code that uses the small-displacement method to generate the force constant matrix.[77] The off-resonant first-order Raman spectra are obtained by using the derivative of the dielectric tensor with respect to the vibrational normal modes. Non-analytical corrections to the longitudinal optical (LO) and transverse optical (TO) phonon branches are applied *via* density functional perturbation theory (DFPT) as implemented in the QUANTUM ESPRESSO package.[78] The non-relativistic Martins–Troullier NORMCONS type pseudopotential[79] in the form of the PBE functional[80] is used for the DFPT calculations.

In order to investigate the optical properties, the complex dielectric function is calculated in order to obtain the excitonic effects by the implementation of the Bethe–Salpeter equation (BSE)[81,82] on top of the quasiparticle energies derived from G_0W_0 approximation with the inclusion of SOC. In the G_0W_0 and BSE steps, the BZ is sampled with a *k*-point grid of 12 × 12 × 1 and the energy cutoff for the response function is taken to be 150 eV. Since the long-range Coulomb interactions dramatically affect the energy of the excitonic states, the vacuum spacing is increased to 25 Å. For the calculations of the excitonic states, the 8 uppermost occupied and 8 lowermost unoccupied states are considered. The refractive index (n), extinction coefficient (κ), and absorption coefficient ($\alpha(w)$) are calculated with the corresponding equations:

$$n = \frac{1}{\sqrt{2}}\left(\varepsilon_1 + \left(\varepsilon_1{}^2 + \varepsilon_2{}^2\right)^{1/2}\right)^{1/2} \tag{2}$$

$$\kappa = \frac{1}{\sqrt{2}}\left(-\varepsilon_1 + \left(\varepsilon_1{}^2 + \varepsilon_2{}^2\right)^{1/2}\right)^{1/2} \tag{3}$$

$$\alpha(w) = \sqrt{2}\omega\left[\left(\varepsilon_1(\omega)^2 + \varepsilon_2(\omega)^2\right)^{1/2} - \varepsilon_1(\omega)\right]^{1/2} \tag{4}$$

where ε_1 and ε_2 are the real and imaginary parts of the complex dielectric function, respectively, and ω is the angular frequency. Reflectance ($R(\omega)$) and transmittance ($T(\omega)$) depend on n and κ, and are defined as

 This journal is © the Partner Organisations 2021

Published on 31 March 2021. Downloaded by Izmir Yuksek Teknoloji on 5/6/2022 8:51:36 AM.

$$R(\omega) = \frac{(n-1)^2 + \kappa^2}{(n+1)^2 + \kappa^2} \tag{5}$$

$$T(\omega) = (1 - R(\omega))^2 e^{-\alpha(w)l}, \tag{6}$$

where l denotes the thickness of the crystal. The exciton binding energy is defined as the difference between the energy of the optical transition and the energy of the fundamental direct band gap between the bands of interest.

3 Results

3.1 Single layers of GaP and GaSe

In this section, the structural, electronic, and vibrational properties of GaP and GaSe single layers are investigated. As shown in Fig. 1(a), GaP crystallizes in a low buckled honeycomb structure where the atomic layers of Ga and P atoms lie in different subplanes separated by a thickness of Δ. On the other hand, single layer GaSe contains two Ga and two Se atoms in a hexagonal primitive cell where the axially aligned Ga atoms are surrounded by trigonally arranged Se atoms, forming a tetralayered atomically thin slab in the array of Se–Ga–Ga–Se. As listed in Table 1, the optimized lattice parameters ($a = b$) of the hexagonal unit cells, calculated to be 3.90 and 3.78 Å for the GaP and GaSe crystals, respectively, are in good agreement with the previously reported theoretical,[34] and experimental[83] results. In GaP, the buckling distance (Δ) between adjacent atoms is 0.44 Å, and the bond length between the Ga and P atoms is 2.29 Å. In GaSe, the distance between the outermost Se atoms indicates that the thickness is 4.83 Å and the bond lengths of the neighboring Ga–Se and Ga–Ga pairs are 2.48 and 2.45 Å, respectively. The calculated cohesive energies per atom for GaP (3.19 eV) and GaSe (3.53 eV) are considerably lower than the reported values for graphene, MoS_2, and h-BN single layers.[34,84,85] While the work function is determined to be 5.64 eV for GaSe, due to the buckled configuration in GaP, the work functions are found to be 4.71 and 5.59 eV for the Ga and P sides, respectively.

As presented in Fig. 1(b), the electronic properties of GaP and GaSe single layers are investigated in the framework of electronic band dispersions through the whole BZ. It is seen that GaP is a semiconductor with an indirect band gap of 2.72 eV, whose valence band maximum (VBM) and conduction band minimum (CBM) are located at the K and Γ high symmetry points, respectively. In addition, the light and heavy hole states at the edge of the Γ point have a split in energy of about 83 meV due to SOC. On the other hand, GaSe is a quasi-direct band gap semiconductor where both direct and indirect transitions are allowed owing to the inverted Mexican hat shaped dispersion of the VB around the zone center. The VBM in GaSe resides between the Γ and K points and is about 64 meV higher in energy than the band edge at the Γ point. The indirect band gap of the structure is calculated to be 2.93 eV. The SOC splitting at the Γ point is determined to be 374 meV. The G_0W_0 quasiparticle band gaps (E_{QP}s) are calculated to be 3.68 and 3.81 eV for GaP and GaSe, respectively.

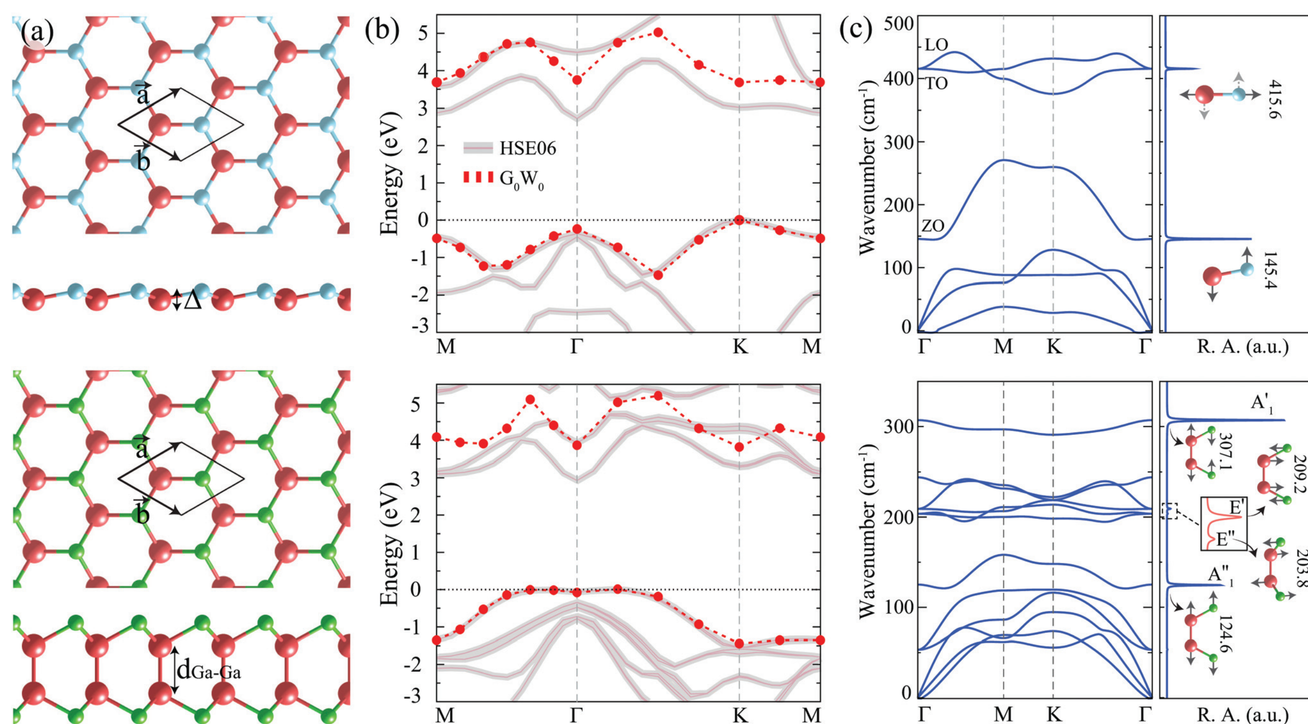

Fig. 1 For the single layers of GaP (top) and GaSe (bottom): (a) top and side views of the atomic structures (the black arrows represent the lattice vectors of the hexagonal primitive cell), (b) HSE06 and G_0W_0 calculated electronic band dispersions, and (c) phonon band dispersions including Raman activity spectra. Red, blue and green colors represent Ga, P and Se atoms, respectively.

Published on 31 March 2021. Downloaded by Izmir Yuksek Teknoloji on 5/6/2022 8:51:36 AM.

Table 1 Calculated parameters of the GaP and GaSe single-layer structures in the ground state: lattice parameters of the primitive cell, $a = b$; bond lengths between Ga and X atoms (X = P or Se), d_{Ga-X}; bond length between Ga atoms, d_{Ga-Ga}; slab thickness, t; buckling distance, Δ; cohesive energy per atom, E_{Coh}; charge transfer to P or Se atoms, $\Delta\rho$; work function, Φ; electronic band gaps calculated using the GGA functionals corrected with SOC + HSE06, E_{gap}^{HSE06}, and SOC + G_0W_0, $E_{gap}^{G_0W_0}$, with high symmetry points indicating where the valence (VBM) and conduction band (CBM) edges are located; LO–TO splitting at the Γ-point, Δ_{LOTO}, exciton binding energy of the first excitonic transition, E_{exc}

	$a{=}b$ (Å)	d_{Ga-X} (Å)	d_{Ga-Ga} (Å)	t (Å)	Δ (Å)	E_{Coh} (eV)	$\Delta\rho$ (e^-)	Φ (eV)	E_{gap}^{HSE06} (eV)	$E_{gap}^{G_0W_0}$ (eV)	Δ_{LOTO} (cm^{-1})	E_{exc} (eV)
GaP	3.90	2.29	—	—	0.44	3.19	0.7	4.71–5.59	2.72/K–Γ	3.68/K–K	33	0.95
GaSe	3.78	2.48	2.45	4.83	—	3.53	0.6	5.64	2.93/ΓK–Γ	3.81/ΓK–K	34	0.65

The vibrational properties of the single layer structures are investigated by calculating the phonon band dispersion and first-order Raman activities (Fig. 1(c)). GaP possesses 3 optical phonon branches. The mode at 145.4 cm^{-1} represents the non-degenerate out-of-plane ZO mode which originates from the anti-phase vibrations of the Ga and P atoms. The highest optical mode, composed of the in-plane longitudinal optical (LO) and transverse optical (TO) modes, is found to be degenerate at 415.6 cm^{-1}; however, upon considering non-analytical terms, the LO and TO modes show splitting (33 cm^{-1}) which is directly related to the polarity of the Ga–P bonds. According to the Raman spectrum of GaP (see Fig. 1(c)), all optical phonon modes display Raman activity in which the ZO mode is the most prominent one. GaSe exhibits 6 optical branches, such that 3 degenerate in-plane and 3 non-degenerate out-of-plane modes are present. Two of the out-of-plane modes, namely A''_1 and A'_1 (at frequencies of 124.6 and 307.1 cm^{-1}, respectively) and two of the in-plane E″ and E′ modes at 203.8 and 209.2 cm^{-1}, respectively, are determined to be Raman active. While A''_1 arises from the anti-phase oscillation of the upper and lower Ga–Se pairs, the A'_1 and E″ modes appear with the inverse motion of each atomic plane. On the other hand, the E′ mode represents the opposite stretching of the Ga and Se atoms. The Raman activity of the in-plane modes is relatively weak compared to the out-of-plane modes. Our results reveal that the non-analytic correction leads to a break in the degeneracy of E′ at the Γ point where the in-plane LO and TO modes split with a frequency of 34 cm^{-1}, and lie at 237 and 203 cm^{-1}, respectively.

3.2 Vertically stacked vdW heterostructures of GaP and GaSe

3.2.1 Structural and phononic properties. In this section, the possible vertical stacking types are investigated to obtain the ground-state configurations of the GaP/GaSe heterobilayer structures. Depending on the buckled structure of GaP, it is essential to consider both situations where Ga or P atoms directly interact with the GaSe layer. Accordingly, we found that 12 different stacking orders are possible between the single layers, as represented in Fig. S1.† While in the group of AA, AA′, AB, AB′, AC and AC′ stacking orders, GaP interacts directly through the Ga atoms with GaSe, their transposed structures of A^TA, A^TA', A^TB, A^TB', A^TC and A^TC' occur with the displacement of buckled Ga atoms with P. The structural optimizations, performed for each type of heterojunction, result in the same lattice parameter of 3.84 Å. Here, the crystal lattices of the GaP and GaSe structures are exposed to biaxial compressive and tensile strains of 1.54% and 1.59%, respectively, as a consequence of their vertical stacking. As shown in Fig. 2(a), AA′ stacking, where Ga atoms reside closer to the top Se atoms, is calculated to be the ground-state configuration as a result of the strong interaction between Ga–Se pairs. As listed in Table 2, the binding energy between the individual layers is 259 meV per unit cell in AA′. When we consider the cases where the P atoms reside closer to the interface, the A^TB' type stacking order is favoured, with a 52 meV higher energy per unit cell than AA′. The interlayer distances (the distance between the uppermost Se and lowermost Ga (P) atomic planes) in the heterobilayers are found to be 2.98 and 3.04 for AA′ and A^TB', respectively.

The stability and the vibrational properties of the AA′ and A^TB' heterobilayers are investigated in terms of the phonon spectrum. As presented in Fig. 2(b), each structure is free from any negative phonon branches through the whole BZ, indicating the stability of each stacked heterobilayer. Obviously, the overall dispersion characteristics of both heterostructures are similar. In AA′ stacking, the frequency of the highest optical phonon branch, corresponding to the LO–TO mode in GaP, is about 9.7 cm^{-1} lower than that of A^TB', since the increased buckling distance, depending on the strong interlayer interactions, weakens the bond strength between the Ga–P pairs. In addition, the splitting in the LO–TO modes of the individual layers reduces with the formation of heterobilayers. This is attributed to the fact that the strong interlayer coupling alters the charge distribution at the interface, which leads to a decrease in the ionic character of the heterobilayers.

The Raman spectra of the heterobilayers are presented in Fig. 2(c) to analyze how the vibrational characteristics vary depending on the stacking order. Within the low-frequency region (between ~0–60 cm^{-1}), A^TB' displays 3 main peaks. The first two peaks, located at 23.1 and 39.4 cm^{-1}, correspond to the non-degenerate shear mode (SM) and doubly degenerate layer breathing mode (LBM) which originate from the in-plane and out-of-plane rigid body motions of the individual layers, respectively. The third one at 53.1 cm^{-1} is composed of the anti-phase motion of the Ga–Se pairs coupled with the GaP layer along the basal plane. In the case of AA′, the SM decreases to 21.9 cm^{-1}, and the LBM vanishes; moreover the mode at 52.8 cm^{-1} is lower in frequency but more prominent compared to that of A^TB'. The Raman intensity enhancement

 This journal is © the Partner Organisations 2021

Published on 31 March 2021. Downloaded by Izmir Yuksek Teknoloji on 5/6/2022 8:51:36 AM.

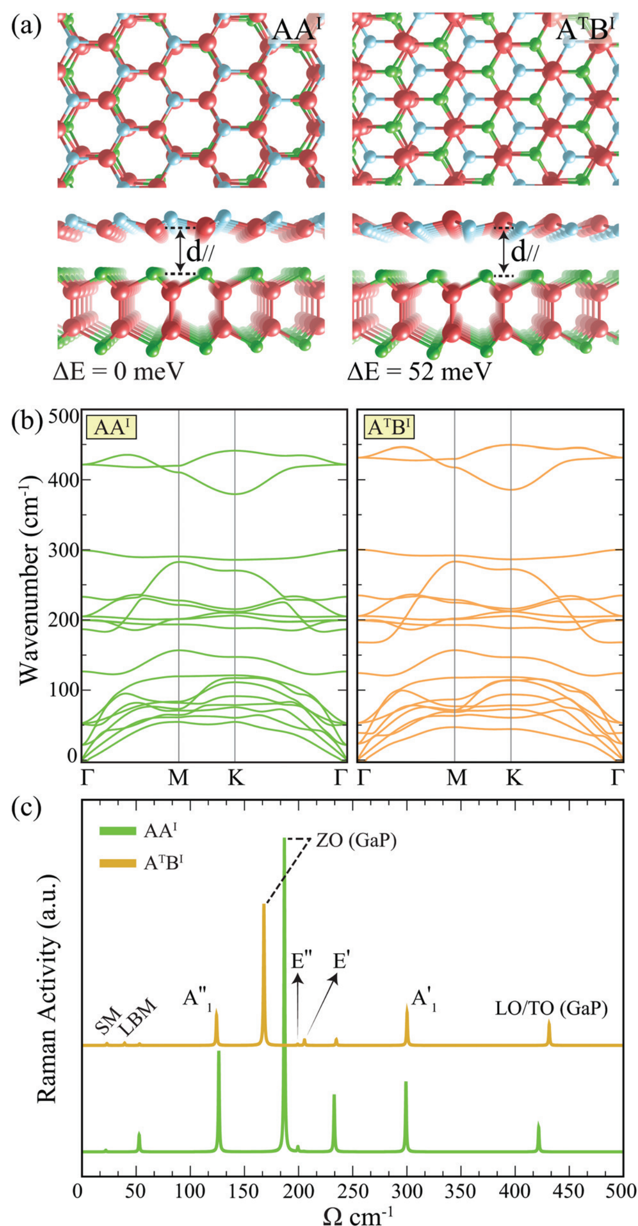

Fig. 2 Top and side views of the optimized atomic structures of AA′ and A^TB' type stacking configurations. (b) Phonon band structures and (c) calculated first order Raman spectra of the considered stacking orders.

Table 2 For the AA′ and A^TB' stacking configurations of the GaP/GaSe heterobilayers: band alignment type; lattice parameters, $a = b$; interlayer distance, $d_{\parallel}$; buckling distance in the GaP layer, Δ; binding energy between layers per unit cell, $E_{binding}$; electronic band gaps calculated within the GGA functional corrected with SOC + G_0W_0 approximation with high symmetry points where the valence (VBM) and conduction band (CBM) edges are located; exciton binding energy, E_{exc}

	Type	$a = b$ (Å)	$d_{\parallel}$ (Å)	Δ (Å)	$E_{binding}$ (meV)	$E_{gap}^{G_0W_0}$ (eV)	E_{exc} (eV)
AA′	II	3.84	2.98	0.55	259	1.78/Γ–Γ	0.35
A^TB'	I	3.84	3.04	0.51	207	2.70/ΓK–M	0.52

in AA′ arises from the strong interlayer coupling that increases the polarizability of the structure.

In the range of 100–350 cm^{-1}, the spectrum is mostly dominated by the characteristic Raman active modes analogous to those of the single layers. The most intense and prominent peak of each spectrum is the ZO mode of GaP at frequencies of 186.9 and 168 cm^{-1} for the AA′ and A^TB' stacking orders, respectively. It is evident that the most precise way to identify the stacking type is directly related to the peak position of the ZO mode. In the AA′ stacking order, the A''_1 mode is located at 126.3 cm^{-1}, and is slightly red-shifted to 124.3 cm^{-1} in A^TB'. In contrast, the A'_1 mode is found at 299.1 cm^{-1} in AA′ and is blue-shifted to 300.2 cm^{-1} in the case of A^TB'. The peaks located at 232.9 and 234.8 cm^{-1}, stemming from the out-of-plane motion of the Ga–Se pairs, are seen only for the heterobilayer structures. Since the peak is considerably more intense in the case of AA′, it can be utilized for the detection of the heterostructure type. The low-intensity peaks at 199.4 and 199.1 cm^{-1} are equivalent to the E″ mode in AA′ and A^TB', respectively. The E′ mode is only observable in A^TB' at a frequency of 205.5 cm^{-1}. Another distinguishable Raman mode based on the stacking configuration is the highest frequency mode that represents LO–TO vibrations in GaP, which is located at 421.8 and 431.5 cm^{-1} for AA′ and A^TB', respectively. Note that each out-of-plane mode arises when the oscillations in individual layers can slightly couple with neighboring layers, whereas the same conclusion is absent for the in-plane modes. Herewith, we conclude that Raman spectroscopy is an efficient tool to confirm the presence of the GaP/GaSe heterostructure and detect the type of stacking configuration.

3.2.2 Stacking dependent electronic and optical properties. As presented in Fig. 3, the electronic properties of the GaP/GaSe heterobilayer vary in the AA′ and A^TB' stacking types, since the asymmetric charge distribution within the atomic planes of GaP enables the alteration of the band alignment according to the buckling orientation of GaP on GaSe. The overlapped electronic states at the interface of AA′ type stacking results in the formation of a type-II heterostructure where the VB and CB possess the dispersion characteristics of GaP and GaSe, respectively. The heterostructure is a direct semiconductor with a E_{QP} of 1.78 eV at the Γ point. Differing from the electronic structure of GaP, the VBM is located at the Γ point, since the shrinkage in the lattice of GaP shifts the VB at the K point to lower levels. On the other hand, A^TB' type stacking forms type-I band alignment where the VB and CB reside in the GaSe layer. For this heterojunction, E_{QP} is calculated to be 2.70 eV.

Electronically, GaP/GaSe heterostructures, which have quite different properties from their components, can be expected to exhibit unique properties in terms of their optical characteristics. Therefore, it is important to understand the absorption, transmission, reflectance and excitonic effects that will occur as a result of the interactions of these possible GaP/GaSe heterostructures with light.

As shown in Fig. 4(a) by the dashed red lines, the quasiparticle bandgaps of the GaP and GaSe single layers are 3.68 and

View Article Online

Published on 31 March 2021. Downloaded by Izmir Yuksek Teknoloji on 5/6/2022 8:51:36 AM.

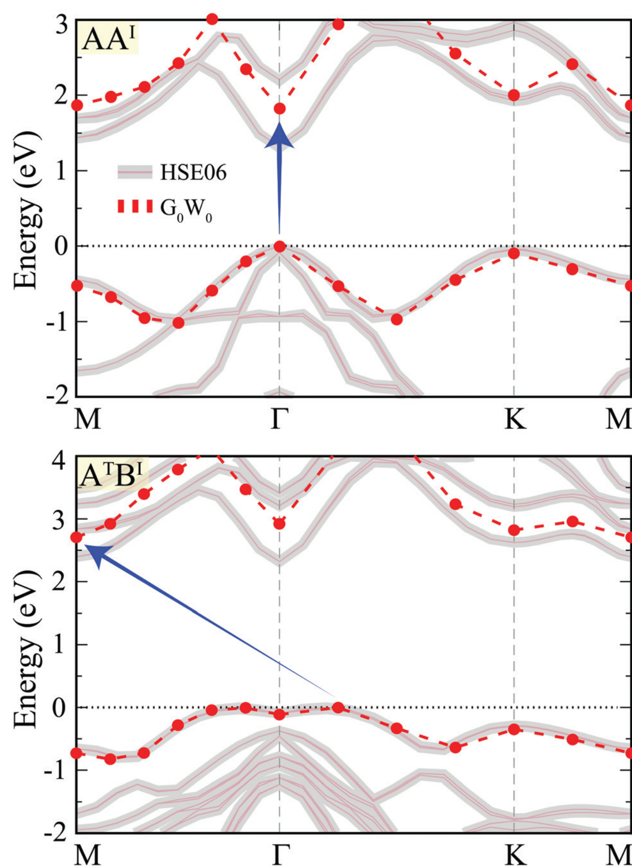

Fig. 3 Electronic band dispersions of the AA′ and A^{T}B′ type stacking configurations of GaP/GaSe heterostructures calculated with the HSE06 functional and G_0W_0 approximation.

3.81 eV, respectively, and their absorption band edges lie within the range of near-UV, indicating the presence of strongly bonded electron and hole pairs. It is apparent that single layer GaP exhibits several bound exciton states in the higher energy portion of the visible spectrum. The first peak at 2.73 eV that exhibits the highest oscillator strength corresponds to the optical transition between the band edges at the K point with a large exciton binding energy (E_{exc}) of 0.95 eV, which is quite close to that reported for single layer MoS_2 (~1.0 eV)[86] and higher than those of black phosphorus (0.70 eV),[87] antimonene (0.8 eV) and arsenene (0.9 eV).[88] In addition, the higher energy peaks at 3.21 and 3.29 eV can be attributed to optical transitions from the heavy and light hole states at the Γ point, respectively, while the peak at 3.06 eV may arise from the direct transitions occurring at the M point or nesting regions.[89] Further characterizations are necessary to clarify the origins of the excitonic transitions in GaP. In the case of the single layer GaSe crystal, the two optical absorption peaks within the UV-A region consist of excitons originating from band-to-band transitions near the zone center or saddle points in between the Γ–M line.[90] Two main excitons are identified within the first absorption peak, such that the transition at 3.30 eV indicates the optical gap, while the second exciton at 3.37 eV is assigned to the first absorption peak because of the stronger oscillator strength. This result is in good agreement with the experimental study, which demonstrates an optical band gap of about 3.30 eV for a graphene-supported single layer of GaSe.[91] The E_{exc} for the lowest exciton, derived from the topmost band-to-band direct transitions near the Γ point,[92] is calculated to be about 0.65 eV.

In addition, for AA′ stacking, one can expect interlayer exciton formation as the charge carriers are spatially separated due to the localization of the electron and hole states in adjacent layers of GaSe and GaP, respectively. The absorption spectrum of the AA′ stacked heterobilayer displays two electronic transitions below the band edge at 1.41 and 1.48 eV. These peaks are attributed to the interlayer excitons composed of the transitions from the spin split states at the Γ point to the conduction band edge, with an identical E_{exc} of 0.38 eV. Due to the spatially independent character of the electron and hole states the oscillator strengths of such transitions are quite small. However, in the case of A^{T}B′, the intense absorption peak at 2.65 eV obviously stems from the electronic transition that takes place in the GaP component of the heterostructure. Consequently, the oscillator strength of this electronic transition, which implies the formation of spatially direct excitons in A^{T}B′, is significantly stronger compared to interlayer transitions in AA′. The E_{exc} for the corresponding peak is 0.52 eV, which is smaller than that of the isolated GaP layer due to the increased screening with the heterobilayer formation.[93]

As shown in Fig. 4(b), the optical transitions are also observable from the reflectance spectra of the single layers. These exciton related reflections in GaP are found to be higher in intensity compared to previously reported results for monolayer MoS_2.[94] The same conclusion is observable for the GaP and GaSe structures since the relatively higher oscillator strengths of optical transitions in GaP lead to stronger reflections. It is also seen that the maximum reflection, about 42%, appears from the lowest energy excitonic state in GaP, while in GaSe, the highest reflectivity values, about 27%, are observed from the optical transitions closest to the absorption band edge. Moreover, it is found that the reflectance and transmittance spectra distinctly vary depending on the stacking type. The reflection is significantly lower below the absorption band edge of AA′, which is in contrast with A^{T}B′ in which the most prominent reflection peak originates from the optical transition with a rate of 37%. In both structures (Fig. 4(c)), the transmission rate is about 80–85% within the lower energy portion of the visible spectrum and starts to decrease gradually until a sharp drop is caused by the first optical transition. Moreover, the excitonic transitions in these single layer crystals can also be monitored from their transmittance spectra. In the transmittance spectrum of AA′, the first two exciton-induced small dips are easily detectable before the sharp drop due to the absorption by bound electrons. On the other hand, the transmission in A^{T}B′ exponentially drops until the excitonic state completely prevents the light transition through the medium. Obviously, depending on the stacking type between the GaP and GaSe layers, the electronic behaviors inside the

 This journal is © the Partner Organisations 2021

Published on 31 March 2021. Downloaded by Izmir Yuksek Teknoloji on 5/6/2022 8:51:36 AM.

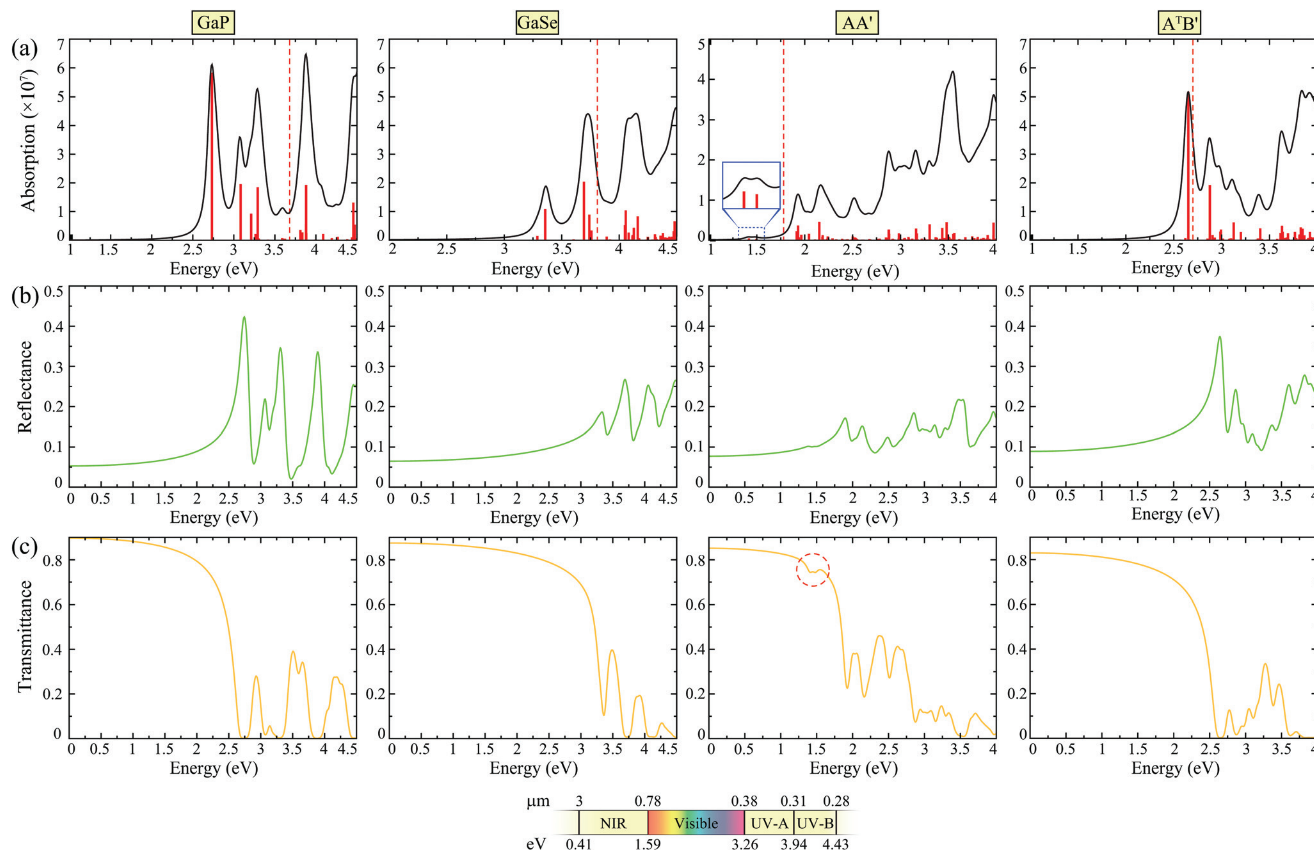

Fig. 4 (a) G_0W_0 + BSE absorption coefficient with the corresponding oscillator strengths (vertical red lines) of the optical transitions, (b) reflectance and (c) transmittance spectra of the GaP and GaSe single layers with their AA′ and A^{T}B′ stacked heterostructures, as a function of photon energy ($\hbar\omega$). The red dashed lines in the absorption spectra refer to the quasiparticle band gaps. The scale bar represents the portion of the electromagnetic spectrum in the range between the near-infrared and near ultraviolet regions.

heterostructures vary and consequently this causes the formation of their distinctive electronic and optical features compared to their individual layers.

4 Conclusions

In summary, by means of density functional based *ab initio* calculations, we have investigated the vibrational and optical characteristics of vertically stacked bilayer heterostructures composed of GaP and GaSe single layers. Phonon calculations have revealed that the corresponding single layers are able to form a dynamically stable crystal environment. We showed that the alignment of the energy states at the interface varies depending on the buckling orientation of GaP on top of GaSe, which induces the formation of type-II or type-I heterojunctions that possess direct and indirect band gaps, respectively. Moreover, each stacking type is found to be distinguishable *via* Raman spectroscopy owing to the significant spectral differences related to the interlayer interactions. The optical properties, determined by the inclusion of electron–hole interactions and excitonic effects, revealed that the type-I and type-II heterostructures display distinctive excitonic absorptions associated with intraband and interband excitations. In addition, these transitions are found to be easily detectable from the transmittance and reflectance spectra of the corresponding heterostructures. We believe that GaP/GaSe heterobilayers demonstrate remarkable properties for use in future photonic and optoelectronic applications.

Conflicts of interest

There are no conflicts to declare.

Acknowledgements

Computational resources were provided by TUBITAK ULAKBIM, at the High Performance and Grid Computing Center (TR-Grid e-Infrastructure). H. S. acknowledges the financial support from the Scientific and Technological Research Council of Turkey (TUBITAK) under the project number 117F095 and from the Turkish Academy of Sciences under the GEBIP program.

Published on 31 March 2021. Downloaded by Izmir Yuksek Teknoloji on 5/6/2022 8:51:36 AM.

References

1 K. S. Novoselov, A. K. Geim, S. V. Morozov, D. Jiang, Y. Zhang, S. V. Dubonos, I. V. Grigorieva and A. A. Firsov, Electric field effect in atomically thin carbon films, *Science*, 2004, **306**(5696), 666–669.

2 K. S. Novoselov, A. K. Geim, S. V. Morozov, D. Jiang, M. I. Katsnelson, I. V. Grigorieva, S. V. Dubonos and A. A. Firsov, Two-dimensional gas of massless Dirac fermions in graphene, *Nature*, 2005, **438**(7065), 197–200.

3 B. Radisavljevic, A. Radenovic, J. Brivio, V. Giacometti and A. Kis, Single-layer MoS_2 transistors, *Nat. Nanotechnol.*, 2011, **6**(3), 147–150.

4 S. Das, H.-Y. Chen, A. V. Penumatcha and J. Appenzeller, High performance multilayer MoS_2 transistors with scandium contacts, *Nano Lett.*, 2013, **13**(1), 100–105.

5 S. Yang, J. Cha, J. C. Kim, D. Lee, W. Huh, Y. Kim, S. W. Lee, H.-G. Park, H. Y. Jeong, S. Hong, G.-H. Lee and C.-H. Lee, Monolithic interface contact engineering to boost optoelectronic performances of 2D semiconductor photovoltaic heterojunctions, *Nano Lett.*, 2020, **20**(4), 2443–2451.

6 N. Flöry, P. Ma, Y. Salamin, A. Emboras, T. Taniguchi, K. Watanabe, J. Leuthold and L. Novotny, Waveguide-integrated van der Waals heterostructure photodetector at telecom wavelengths with high speed and high responsivity, *Nat. Nanotechnol.*, 2020, **15**(2), 118–124.

7 A. Pospischil, M. M. Furchi and T. Mueller, Solar-energy conversion and light emission in an atomic monolayer p–n diode, *Nat. Nanotechnol.*, 2014, **9**(4), 257–261.

8 J. Liu, X. Chen, Q. Wang, M. Xiao, D. Zhong, W. Sun, G. Zhang and Z. Zhang, Ultrasensitive monolayer MoS_2 field-effect transistor based DNA sensors for screening of down syndrome, *Nano Lett.*, 2019, **19**(3), 1437–1444.

9 A. Splendiani, L. Sun, Y. Zhang, T. Li, J. Kim, C.-Y. Chim, G. Galli and F. Wang, Emerging photoluminescence in monolayer MoS_2, *Nano Lett.*, 2010, **10**(4), 1271–1275.

10 L. Su, X. Fan, T. Yin, H. Wang, Y. Li, F. Liu, J. Li, H. Zhang and H. Xie, Inorganic 2D luminescent materials: structure, luminescence modulation, and applications, *Adv. Opt. Mater.*, 2020, **8**(1), 1900978.

11 K. S. Novoselov, D. Jiang, F. Schedin, T. Booth, V. V. Khotkevich, S. Morozov and A. K. Geim, Two-dimensional atomic crystals, *Proc. Natl. Acad. Sci. U. S. A.*, 2005, **102**(30), 10451–10453.

12 M. Yi and Z. Shen, A review on mechanical exfoliation for the scalable production of graphene, *J. Mater. Chem. A*, 2015, **3**(22), 11700–11715.

13 L. Ottaviano, S. Palleschi, F. Perrozzi, G. D'Olimpio, F. Priante, M. Donarelli, P. Benassi, M. Nardone, M. Gonchigsuren, M. Gombosuren, A. Lucia, G. Moccia and A. Cacioppo, Mechanical exfoliation and layer number identification of MoS_2 revisited, *2D Mater.*, 2017, **4**(4), 045013.

14 H. Yu, M. Liao, W. Zhao, G. Liu, X. Zhou, Z. Wei, X. Xu, K. Liu, Z. Hu, K. Deng, S. Zhou, J.-A. Shi, L. Gu, C. Shen, T. Zhang, L. Du, L. Xie, J. Zhu, W. Chen, R. Yang, D. Shi and G. Zhang, Wafer-scale growth and transfer of highly-oriented monolayer MoS_2 continuous films, *ACS Nano*, 2017, **11**(12), 12001–12007.

15 D. Dumcenco, D. Ovchinnikov, K. Marinov, P. Lazic, M. Gibertini, N. Marzari, O. L. Sanchez, Y.-C. Kung, D. Krasnozhon, M.-W. Chen, S. Bertolazzi, P. Gillet, A. Fontcuberta i Morral, A. Radenovic and A. Kis, Large-area epitaxial monolayer MoS_2, *ACS Nano*, 2015, **9**(4), 4611–4620.

16 Q. Wang, N. Li, J. Tang, J. Zhu, Q. Zhang, Q. Jia, Y. Lu, Z. Wei, H. Yu, Y. Zhao, Y. Guo, L. Gu, G. Sun, W. Yang, R. Yang, D. Shi and G. Zhang, Wafer-scale highly oriented monolayer MoS_2 with large domain sizes, *Nano Lett.*, 2020, **20**(10), 7193–7199.

17 V. Sreepal, M. Yagmurcukardes, K. S. Vasu, D. J. Kelly, S. F. Taylor, V. G. Kravets, Z. Kudrynskyi, Z. D. Kovalyuk, A. Patanè, A. N. Grigorenko, S. J. Haigh, C. Hardacre, L. Eaves, H. Sahin, A. K. Geim, F. M. Peeters and R. R. Nair, Two-dimensional covalent crystals by chemical conversion of thin van der Waals materials, *Nano Lett.*, 2019, **19**(9), 6475–6481.

18 M. Yagmurcukardes, Monolayer fluoro-InSe: Formation of a thin monolayer *via* fluorination of InSe, *Phys. Rev. B*, 2019, **100**(2), 024108.

19 E. D. Kosten, J. H. Atwater, J. Parsons, A. Polman and H. A. Atwater, Highly efficient GaAs solar cells by limiting light emission angle, *Light: Sci. Appl.*, 2013, **2**(1), e45.

20 H. Lim, J. L. Young, J. F. Geisz, D. J. Friedman, T. G. Deutsch and J. Yoon, High performance III–V photoelectrodes for solar water splitting *via* synergistically tailored structure and stoichiometry, *Nat. Commun.*, 2019, **10**(1), 1.

21 Y. Zhang, D. Saxena, M. Aagesen and H. Liu, Toward electrically driven semiconductor nanowire lasers, *Nanotechnology*, 2019, **30**(19), 192002.

22 L.-B. Luo, J.-J. Chen, M.-Z. Wang, H. Hu, C.-Y. Wu, Q. Li, L. Wang, J.-A. Huang and F.-X. Liang, Near-infrared light photovoltaic detector based on GaAs nanocone array/monolayer graphene Schottky junction, *Adv. Funct. Mater.*, 2014, **24**(19), 2794–2800.

23 G. Mariani, A. C. Scofield, C.-H. Hung and D. L. Huffaker, GaAs nanopillar-array solar cells employing *in situ* surface passivation, *Nat. Commun.*, 2013, **4**(1), 1–8.

24 X. Dai, S. Zhang, Z. Wang, G. Adamo, H. Liu, Y. Huang, C. Couteau and C. Soci, GaAs/AlGaAs nanowire photodetector, *Nano Lett.*, 2014, **14**(5), 2688–2693.

25 J. Sun, M. Han, Y. Gu, Z.-x. Yang and H. Zeng, Recent advances in group III–V nanowire infrared detectors, *Adv. Opt. Mater.*, 2018, **6**(18), 1800256.

26 H. Ali, Y. Zhang, J. Tang, K. Peng, S. Sun, Y. Sun, F. Song, A. Falak, S. Wu, C. Qian, M. Wang, Z. Zuo, K. Jin, A. M. Sanchez, H. Liu and X. Xu, High-responsivity photodetection by a self-catalyzed phase-pure p-GaAs nanowire, *Small*, 2018, **14**(17), 1704429.

This journal is © the Partner Organisations 2021

View Article Online

Published on 31 March 2021. Downloaded by Izmir Yuksek Teknoloji on 5/6/2022 8:51:36 AM.

27 C. Zhou, X.-T. Zhang, K. Zheng, P.-P. Chen, W. Lu and J. Zou, Self-assembly growth of In-rich InGaAs core–shell structured nanowires with remarkable near-infrared photoresponsivity, *Nano Lett.*, 2017, **17**(12), 7824–7830.

28 S. Assali, I. Zardo, S. Plissard, D. Kriegner, M. A. Verheijen, G. Bauer, A. Meijerink, A. Belabbes, F. Bechstedt, J. E. M. Haverkort and E. P. A. M. Bakkers, Direct band gap wurtzite gallium phosphide nanowires, *Nano Lett.*, 2013, **13**(4), 1559–1563.

29 G. Benz and R. Conradt, Auger recombination in GaAs and GaSb, *Phys. Rev. B: Solid State*, 1977, **16**(2), 843.

30 C. M. Wolfe, G. Stillman and W. Lindley, Electron mobility in high-purity GaAs, *J. Appl. Phys.*, 1970, **41**(7), 3088–3091.

31 A. Konar, J. Mathew, K. Nayak, M. Bajaj, R. K. Pandey, S. Dhara, K. Murali and M. M. Deshmukh, Carrier transport in high mobility InAs nanowire junctionless transistors, *Nano Lett.*, 2015, **15**(3), 1684–1690.

32 C. Thomas, A. Hatke, A. Tuaz, R. Kallaher, T. Wu, T. Wang, R. Diaz, G. Gardner, M. Capano and M. Manfra, High-mobility InAs 2DEGs on GaSb substrates: A platform for mesoscopic quantum transport, *Phys. Rev. Mater.*, 2018, **2**(10), 104602.

33 X. Jiang, Q. Xiong, S. Nam, F. Qian, Y. Li and C. M. Lieber, InAs/InP radial nanowire heterostructures as high electron mobility devices, *Nano Lett.*, 2007, **7**(10), 3214–3218.

34 H. Şahin, S. Cahangirov, M. Topsakal, E. Bekaroglu, E. Akturk, R. T. Senger and S. Ciraci, Monolayer honeycomb structures of group-IV elements and III–V binary compounds: First-principles calculations, *Phys. Rev. B: Condens. Matter Mater. Phys.*, 2009, **80**(15), 155453.

35 Y. Chen, J. Liu, M. Zeng, F. Lu, T. Lv, Y. Chang, H. Lan, B. Wei, R. Sun, J. Gao, Z. Wang and L. Fu, Universal growth of ultra-thin III–V semiconductor single crystals, *Nat. Commun.*, 2020, **11**(1), 1.

36 M. Pilkuhn and L. Foster, Green luminescence from solution-grown junctions in GaP containing shallow donors and acceptors, *IBM J. Res. Dev.*, 1966, **10**(2), 122–129.

37 J. Cambiasso, G. Grinblat, Y. Li, A. Rakovich, E. Cortés and S. A. Maier, Bridging the gap between dielectric nanophotonics and the visible regime with effectively lossless gallium phosphide antennas, *Nano Lett.*, 2017, **17**(2), 1219–1225.

38 G. Grinblat, M. P. Nielsen, P. Dichtl, Y. Li, R. F. Oulton and S. A. Maier, Ultrafast sub-30 fs all-optical switching based on gallium phosphide, *Sci. Adv.*, 2019, **5**(6), eaaw3262.

39 V. Remesh, G. Grinblat, Y. Li, S. A. Maier and N. F. van Hulst, Coherent multiphoton control of gallium phosphide nanodisk resonances, *ACS Photonics*, 2019, **6**(10), 2487–2491.

40 D. J. Wilson, K. Schneider, S. Hönl, M. Anderson, Y. Baumgartner, L. Czornomaz, T. J. Kippenberg and P. Seidler, Integrated gallium phosphide nonlinear photonics, *Nat. Photonics*, 2020, **14**(1), 57–62.

41 B. P. Bahuguna, L. Saini, R. O. Sharma and B. Tiwari, Strain and electric field induced metallization in the GaX (X = N, P, As & Sb) monolayer, *Phys. E*, 2018, **99**, 236–243.

42 N. C. Fernelius, Properties of gallium selenide single crystal, *Prog. Cryst. Growth Charact. Mater.*, 1994, **28**(4), 275–353.

43 A. Segura, J. Bouvier, M. Andrés, F. Manjón and V. Munoz, Strong optical nonlinearities in gallium and indium selenides related to inter-valence-band transitions induced by light pulses, *Phys. Rev. B: Condens. Matter Mater. Phys.*, 1997, **56**(7), 4075.

44 Y. Zhou, Y. Nie, Y. Liu, K. Yan, J. Hong, C. Jin, Y. Zhou, J. Yin, Z. Liu and H. Peng, Epitaxy and photoresponse of two-dimensional GaSe crystals on flexible transparent mica sheets, *ACS Nano*, 2014, **8**(2), 1485–1490.

45 T. Afaneh, A. Fryer, Y. Xin, R. H. Hyde, N. Kapuruge and H. R. Gutiérrez, Large-area growth and stability of monolayer gallium monochalcogenides for optoelectronic devices, *ACS Appl. Nano Mater.*, 2020, **3**(8), 7879–7887.

46 P. Hu, Z. Wen, L. Wang, P. Tan and K. Xiao, Synthesis of few-layer GaSe nanosheets for high performance photodetectors, *ACS Nano*, 2012, **6**(7), 5988–5994.

47 S. Lei, L. Ge, Z. Liu, S. Najmaei, G. Shi, G. You, J. Lou, R. Vajtai and P. M. Ajayan, Synthesis and photoresponse of large GaSe atomic layers, *Nano Lett.*, 2013, **13**(6), 2777–2781.

48 H. Arora, Y. Jung, T. Venanzi, K. Watanabe, T. Taniguchi, R. Hübner, H. Schneider, M. Helm, J. C. Hone and A. Erbe, Effective hexagonal boron nitride passivation of few-layered InSe and GaSe to enhance their electronic and optical properties, *ACS Appl. Mater. Interfaces*, 2019, **11**(46), 43480–43487.

49 D. Rybkovskiy, N. Arutyunyan, A. Orekhov, I. Gromchenko, I. Vorobiev, A. Osadchy, E. Y. Salaev, T. Baykara, K. Allakhverdiev and E. Obraztsova, Size-induced effects in gallium selenide electronic structure: The influence of interlayer interactions, *Phys. Rev. B: Condens. Matter Mater. Phys.*, 2011, **84**(8), 085314.

50 H. Cai, J. Kang, H. Sahin, B. Chen, A. Suslu, K. Wu, F. Peeters, X. Meng and S. Tongay, Exciton pumping across type-I gallium chalcogenide heterojunctions, *Nanotechnology*, 2016, **27**(6), 065203.

51 M. Yagmurcukardes, R. Senger, F. Peeters and H. Sahin, Mechanical properties of monolayer GaS and GaSe crystals, *Phys. Rev. B*, 2016, **94**(24), 245407.

52 D. Maeso, S. Pakdel, H. Santos, N. Agraït, J. J. Palacios, E. Prada and G. Rubio-Bollinger, Strong modulation of optical properties in rippled 2D GaSe *via* strain engineering, *Nanotechnology*, 2019, **30**(24), 24LT01.

53 M. Mahjouri-Samani, R. Gresback, M. Tian, K. Wang, A. A. Puretzky, C. M. Rouleau, G. Eres, I. N. Ivanov, K. Xiao, M. A. McGuire, G. Duscher and D. B. Geohegan, Pulsed laser deposition of photoresponsive two-dimensional GaSe nanosheet networks, *Adv. Funct. Mater.*, 2014, **24**(40), 6365–6371.

54 T. Jia, H.-R. Fuh, D. Chen, M. Abid, M. Abid, D. Zhang, A. B. Sarker, J. Cho, M. Choi, B. S. Chun, H. Xu, C. Ó Coileáin, H. Liu, C. Chang and H. Wu, Giant and linear

Published on 31 March 2021. Downloaded by Izmir Yuksek Teknoloji on 5/6/2022 8:51:36 AM.

piezo-phototronic response in layered GaSe nanosheets, *Adv. Electron. Mater.*, 2018, **4**(4), 1700447.
55 X. Zhou, J. Cheng, Y. Zhou, T. Cao, H. Hong, Z. Liao, S. Wu, H. Peng, K. Liu and D. Yu, Strong second-harmonic generation in atomic layered GaSe, *J. Am. Chem. Soc.*, 2015, **137**(25), 7994–7997.
56 A. K. Geim and I. V. Grigorieva, van der Waals heterostructures, *Nature*, 2013, **499**(7459), 419–425.
57 K. Novoselov, A. Mishchenko, A. Carvalho and A. H. C. Neto, 2D materials and van der Waals heterostructures, *Science*, 2016, **353**(6298), aac9439.
58 Y. Liu, N. O. Weiss, X. Duan, H.-C. Cheng, Y. Huang and X. Duan, van der Waals heterostructures and devices, *Nat. Rev. Mater.*, 2016, **1**(9), 16042.
59 A. Chaves, J. Azadani, H. Alsalman, D. R. da Costa, R. Frisenda, A. Chaves, S. H. Song, Y. Kim, D. He, J. Zhou, A. Castellanos-Gomez, F. M. Peeters, Z. Liu, C. L. Hinkle, S.-H. Oh, P. D. Ye, S. J. Koester, Y. H. Lee, P. Avouris, X. Wang and T. Low, Bandgap engineering of two-dimensional semiconductor materials, *npj 2D Mater. Appl.*, 2020, **4**(1), 1–21.
60 X. Hong, J. Kim, S.-F. Shi, Y. Zhang, C. Jin, Y. Sun, S. Tongay, J. Wu, Y. Zhang and F. Wang, Ultrafast charge transfer in atomically thin MoS_2/WS_2 heterostructures, *Nat. Nanotechnol.*, 2014, **9**(9), 682–686.
61 P. Rivera, J. R. Schaibley, A. M. Jones, J. S. Ross, S. Wu, G. Aivazian, P. Klement, K. Seyler, G. Clark, N. J. Ghimire, J. Yan, D. G. Mandrus, W. Yao and X. Xu, Observation of long-lived interlayer excitons in monolayer $MoSe_2$–WSe_2 heterostructures, *Nat. Commun.*, 2015, **6**(1), 6242.
62 E. Calman, M. Fogler, L. Butov, S. Hu, A. Mishchenko and A. Geim, Indirect excitons in van der Waals heterostructures at room temperature, *Nat. Commun.*, 2018, **9**(1), 1895.
63 B. Miller, A. Steinhoff, B. Pano, J. Klein, F. Jahnke, A. Holleitner and U. Wurstbauer, Long-lived direct and indirect interlayer excitons in van der Waals heterostructures, *Nano Lett.*, 2017, **17**(9), 5229–5237.
64 J. Kunstmann, F. Mooshammer, P. Nagler, A. Chaves, F. Stein, N. Paradiso, G. Plechinger, C. Strunk, C. Schüller, G. Seifert, D. R. Reichman and T. Korn, Momentum-space indirect interlayer excitons in transition-metal dichalcogenide van der Waals heterostructures, *Nat. Phys.*, 2018, **14**(8), 801–805.
65 Z. He, J. Guo, S. Li, Z. Lei, L. Lin, Y. Ke, W. Jie, T. Gong, Y. Lin, T. Cheng, W. Huang and X. Zhang, GaSe/MoS_2 heterostructure with ohmic-contact electrodes for fast, broadband photoresponse, and self-driven photodetectors, *Adv. Mater. Interfaces*, 2020, **7**(9), 1901848.
66 R. Lu, J. Liu, H. Luo, V. Chikan and J. Z. Wu, Graphene/GaSe-nanosheet hybrid: towards high gain and fast photoresponse, *Sci. Rep.*, 2016, **6**, 19161.
67 G. Kresse and J. Hafner, *Ab initio* molecular dynamics for liquid metals, *Phys. Rev. B: Condens. Matter Mater. Phys.*, 1993, **47**(1), 558.
68 G. Kresse and J. Furthmüller, Efficient iterative schemes for *ab initio* total-energy calculations using a plane-wave basis set, *Phys. Rev. B: Condens. Matter Mater. Phys.*, 1996, **54**(16), 11169.
69 G. Kresse and D. Joubert, From ultrasoft pseudopotentials to the projector augmented-wave method, *Phys. Rev. B: Condens. Matter Mater. Phys.*, 1999, **59**(3), 1758.
70 P. E. Blöchl, Projector augmented-wave method, *Phys. Rev. B: Condens. Matter Mater. Phys.*, 1994, **50**(24), 17953.
71 J. P. Perdew, K. Burke and M. Ernzerhof, Generalized gradient approximation made simple, *Phys. Rev. Lett.*, 1996, **77**(18), 3865.
72 S. Grimme, S. Ehrlich and L. Goerigk, Effect of the damping function in dispersion corrected density functional theory, *J. Comput. Chem.*, 2011, **32**(7), 1456–1465.
73 J. Heyd, G. E. Scuseria and M. Ernzerhof, Hybrid functionals based on a screened coulomb potential, *J. Chem. Phys.*, 2003, **118**(18), 8207–8215.
74 L. Hedin, New method for calculating the one-particle green's function with application to the electron-gas problem, *Phys. Rev.*, 1965, **139**(3A), A796.
75 M. S. Hybertsen and S. G. Louie, Electron correlation in semiconductors and insulators: Band gaps and quasiparticle energies, *Phys. Rev. B: Condens. Matter Mater. Phys.*, 1986, **34**(8), 5390.
76 M. Shishkin and G. Kresse, Implementation and performance of the frequency-dependent GW method within the PAW framework, *Phys. Rev. B: Condens. Matter Mater. Phys.*, 2006, **74**(3), 035101.
77 A. Togo, F. Oba and I. Tanaka, First-principles calculations of the ferroelastic transition between rutile-type and $CaCl_2$-type SiO_2 at high pressures, *Phys. Rev. B: Condens. Matter Mater. Phys.*, 2008, **78**(13), 134106.
78 P. Giannozzi, S. Baroni, N. Bonini, M. Calandra, R. Car, C. Cavazzoni, D. Ceresoli, G. L. Chiarotti, M. Cococcioni, I. Dabo, A. D. Corso, S. d. Gironcoli, S. Fabris, G. Fratesi, R. Gebauer, U. Gerstmann, C. Gougoussis, A. Kokalj, M. Lazzeri, L. Martin-Samos, N. Marzari, F. Mauri, R. Mazzarello, S. Paolini, A. Pasquarello, L. Paulatto, C. Sbraccia, S. Scandolo, G. Sclauzero, A. P. Seitsonen, A. Smogunov, P. Umari and R. M. Wentzcovitch, QUANTUM ESPRESSO: a modular and open-source software project for quantum simulations of materials, *J. Phys.: Condens. Matter*, 2009, **21**(39), 395502.
79 N. Troullier and J. L. Martins, Efficient pseudopotentials for plane-wave calculations, *Phys. Rev. B: Condens. Matter Mater. Phys.*, 1991, **43**(3), 1993.
80 J. P. Perdew, K. Burke and M. Ernzerhof, Generalized gradient approximation made simple, *Phys. Rev. Lett.*, 1996, **77**(18), 3865.
81 E. E. Salpeter and H. A. Bethe, A relativistic equation for bound-state problems, *Phys. Rev.*, 1951, **84**(6), 1232.
82 W. Hanke and L. Sham, Many-particle effects in the optical spectrum of a semiconductor, *Phys. Rev. B: Condens. Matter Mater. Phys.*, 1980, **21**(10), 4656.

 This journal is © the Partner Organisations 2021

Published on 31 March 2021. Downloaded by Izmir Yuksek Teknoloji on 5/6/2022 8:51:36 AM.

83 X. Li, M.-W. Lin, J. Lin, B. Huang, A. A. Puretzky, C. Ma, K. Wang, W. Zhou, S. T. Pantelides, M. Chi, I. Kravchenko, J. Fowlkes, C. M. Rouleau, D. B. Geohegan and K. Xiao, Two-dimensional GaSe/$MoSe_2$ misfit bilayer heterojunctions by van der Waals epitaxy, *Sci. Adv.*, 2016, **2**(4), e1501882.

84 C. Ataca, M. Topsakal, E. Akturk and S. Ciraci, A comparative study of lattice dynamics of three-and two-dimensional MoS_2, *J. Phys. Chem. C*, 2011, **115**(33), 16354–16361.

85 A. Janotti, S.-H. Wei and D. Singh, First-principles study of the stability of BN and C, *Phys. Rev. B: Condens. Matter Mater. Phys.*, 2001, **64**(17), 174107.

86 D. Y. Qiu, H. Felipe and S. G. Louie, Optical spectrum of MoS_2: many-body effects and diversity of exciton states, *Phys. Rev. Lett.*, 2013, **111**(21), 216805.

87 X. Wang, A. M. Jones, K. L. Seyler, V. Tran, Y. Jia, H. Zhao, H. Wang, L. Yang, X. Xu and F. Xia, Highly anisotropic and robust excitons in monolayer black phosphorus, *Nat. Nanotechnol.*, 2015, **10**(6), 517–521.

88 Y. Wang, P. Huang, M. Ye, R. Quhe, Y. Pan, H. Zhang, H. Zhong, J. Shi and J. Lu, Many-body effect, carrier mobility, and device performance of hexagonal arsenene and antimonene, *Chem. Mater.*, 2017, **29**(5), 2191–2201.

89 S. Gupta, S. N. Shirodkar, A. Kutana and B. I. Yakobson, In pursuit of 2D materials for maximum optical response, *ACS Nano*, 2018, **12**(11), 10880–10889.

90 G. Antonius, D. Y. Qiu and S. G. Louie, Orbital symmetry and the optical response of single-layer MX monochalcogenides, *Nano Lett.*, 2018, **18**(3), 1925–1929.

91 Z. B. Aziza, D. Pierucci, H. Henck, M. G. Silly, C. David, M. Yoon, F. Sirotti, K. Xiao, M. Eddrief, J.-C. Girard and A. Ouerghi, Tunable quasiparticle band gap in few-layer GaSe/graphene van der Waals heterostructures, *Phys. Rev. B*, 2017, **96**(3), 035407.

92 Z. B. Aziza, V. Zólyomi, H. Henck, D. Pierucci, M. G. Silly, J. Avila, S. J. Magorrian, J. Chaste, C. Chen, M. Yoon, K. Xiao, F. Sirotti, M. C. Asensio, E. Lhuillier, M. Eddrief, V. I. Fal'ko and A. Ouerghi, Valence band inversion and spin-orbit effects in the electronic structure of monolayer GaSe, *Phys. Rev. B*, 2018, **98**(11), 115405.

93 S. Ovesen, S. Brem, C. Linderälv, M. Kuisma, T. Korn, P. Erhart, M. Selig and E. Malic, Interlayer exciton dynamics in van der Waals heterostructures, *Commun. Phys.*, 2019, **2**(1), 1–8.

94 Y. Niu, S. Gonzalez-Abad, R. Frisenda, P. Marauhn, M. Drüppel, P. Gant, R. Schmidt, N. S. Taghavi, D. Barcons, A. J. Molina-Mendoza, S. M. D. Vasconcellos, R. Bratschitsch, D. P. D. Lara, M. Rohlfing and A. Castellanos-Gomez, Thickness-dependent differential reflectance spectra of monolayer and few-layer MoS_2, $MoSe_2$, WS_2 and WSe_2, *Nanomaterials*, 2018, **8**(9), 725.